

Cytoskeletal remodelling and slow dynamics in the living cell

PREDRAG BURSAC^{1*}, GUILLAUME LENORMAND^{1*}, BEN FABRY², MADAVI OLIVER¹, DAVID A. WEITZ³, VIRGILE VIASNOFF⁴, JAMES P. BUTLER^{1,5} AND JEFFREY J. FREDBERG^{1†}

¹Physiology Program, School of Public Health, Harvard University, Boston, Massachusetts, 02115, USA

²University of Erlangen-Nuremberg, Institute of Biomedical Technology, D-91054, Erlangen, Germany

³Division of Engineering and Applied Sciences, Harvard University, Cambridge, Massachusetts, 02138, USA

⁴Rowland Institute for Science, Harvard University, Cambridge, Massachusetts, 02142, USA

⁵Department of Geriatric and Respiratory Medicine, Tohoku University School of Medicine, Sendai 980-8574, Japan

*These authors contributed equally to this work

†e-mail: jfredber@hsph.harvard.edu

Published online: 5 June 2005; doi:10.1038/nmat1404

The cytoskeleton (CSK) is a crowded network of structural proteins that stabilizes cell shape and drives cell motions. Recent studies on the dynamics of the CSK have established that a wide variety of cell types exhibit rheology in which responses are not tied to any particular relaxation times and are thus scale-free^{1–4}. Scale-free rheology is often found in a class of materials called soft glasses⁵, but not all materials expressing scale-free rheology are glassy (see plastics, wood, concrete or some metals for example)⁶. As such, the extent to which dynamics of the CSK might be regarded as glassy remained an open question. Here we report both forced and spontaneous motions of microbeads tightly bound to the CSK of human muscle cells. Large oscillatory shear fluidized the CSK matrix, which was followed by slow scale-free recovery of rheological properties (aging). Spontaneous bead motions were subdiffusive at short times but superdiffusive at longer times; intermittent motions reflecting nanoscale CSK rearrangements depended on both the approach to kinetic arrest and energy release due to ATP hydrolysis. Aging, intermittency, and approach to kinetic arrest establish a striking analogy between the behaviour of the living CSK and that of inert non-equilibrium systems, including soft glasses, but with important differences that are highly ATP-dependent. These mesoscale dynamics link integrative CSK functions to underlying molecular events, and represent an important intersection of topical issues in condensed matter physics and systems biology.

The dynamics of soft glassy systems are illustrated most simply in a crowded colloidal suspension⁷, although similar dynamics can arise from other physical interactions, such as attractive interactions or weak chemical bonding. With sufficient crowding, particles can become trapped by their surrounding neighbours. Because these neighbours act as a cage, particle motions are localized most of the time, although occasionally a particle escapes its trap and thus causes the local micro-configuration to rearrange (remodelling). Trapping in such out-of-equilibrium systems arises due to the insufficiency of thermal energy to drive structural rearrangements. With time, however, the system will jump from one metastable state to another, and evolve into micro-configurations that are more and more stable,

but more slowly than any exponential process⁸. Slowly evolving dynamics of this kind is called aging^{9–11}. In such systems, applying a sufficiently large oscillatory shear can provide an additional energy source that can overcome energy barriers, resolve constraints, and drive structural rearrangements. As a consequence, material properties return to their earlier values. In this way aging is reversed and the system is rejuvenated^{9–11}.

We assessed aging in the human airway smooth muscle (HASM) cell as follows. When subjected to a step increase of stress, ongoing material deformation in time, t , is called creep, $J(t)$. We measured changes of $J(t)$ with different waiting times, t_w , the interval from cessation of a large oscillatory shear to the onset of the step increase of stress (Fig. 1a). $J(t, t_w)$ was scale-free⁴, increasing with t as a weak power law, the exponent of which was independent of t_w (Fig. 1b). $J(t, t_w)$ decreased with t_w , showing that the system became progressively stiffer with increasing t_w . For each t_w , we defined τ as the time t at which J crossed an arbitrary threshold (0.5 nm Pa^{-1}). τ showed a biphasic response with t_w , the latter phase of which ($t_w \geq 1,600 \text{ s}$) was unrelated to the applied oscillatory torque (Fig. 1c). For the smaller shear-responsive early phase, time was rescaled⁹ using $t_\mu = t/t_w^\mu$ with an aging exponent $\mu = 0.4$, whereupon all data collapsed onto a unifying master curve (Fig. 1c, inset). Collapse of this kind with aging exponents in the neighbourhood of 0.4 is typical of soft glassy systems that are aging^{12,13}. In contrast, time-control experiments, where no shear was applied, showed a nearly constant τ for $t_w < 1,200 \text{ s}$ (Fig. 1c).

To assess the ability of shear to rejuvenate the system, we measured the dependence of the creep response on the amplitude of the oscillatory torque (Fig. 1d). As the amplitude progressively increased, creep measured on cessation of the oscillatory torque increased as well, indicating partial rejuvenation, but for torque amplitudes $>125 \text{ Pa}$ exhibited a plateau. Importantly, when a second large oscillatory torque was applied 400 s after the first, creep was brought back to within 92% of the value after the first shear, further confirming the ability of shear to rejuvenate the system and to reverse aging (data not shown).

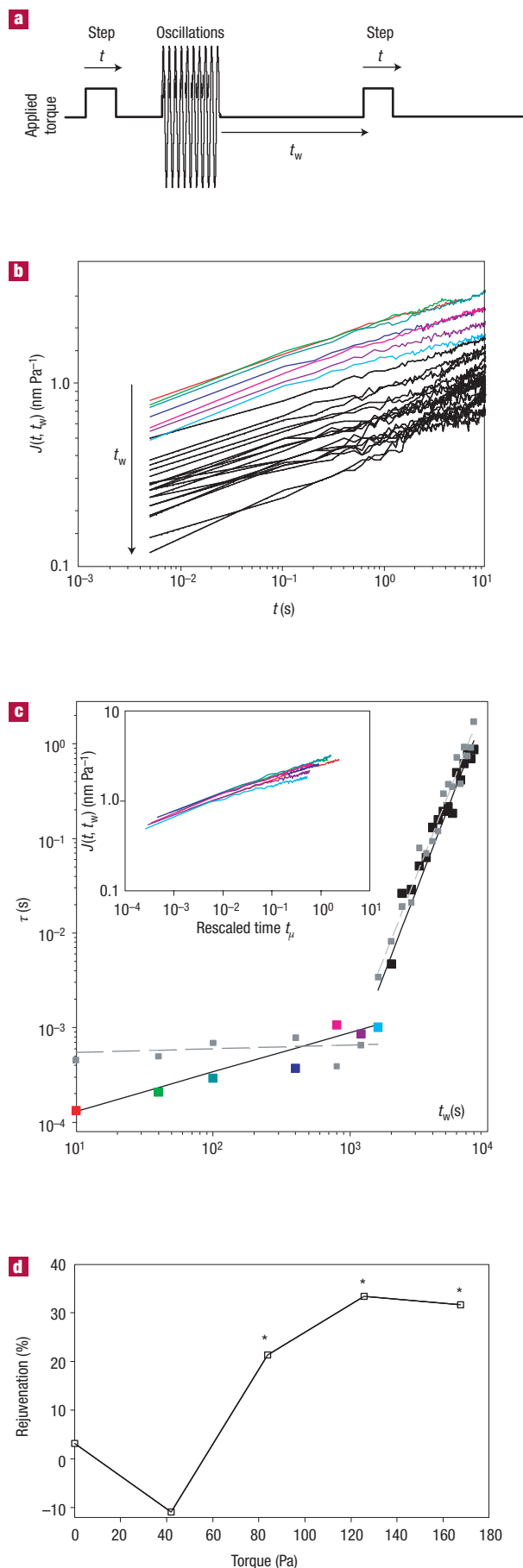


Figure 1 Aging and rejuvenation in response to applied shear. **a**, Applied torque history. **b**, Creep functions at different t_w (each line is median of over 658 beads on a like number of cells): 10 s (red), 40 s (green), 100 s (dark cyan), 400 s (blue), 800 s (pink), 1,200 s (dark pink), 1,600 s (cyan) and every 400 s up to 8,000 s (black). The geometric standard deviation for each $J(t, t_w)$ ranged between 1.2 and 1.5. **c**, Behaviour of τ with waiting time t_w . Colour coding the same as above. Solid lines are best fits by a power law, the exponent of which gives the aging exponent $\mu = 0.4$ for $t_w \leq 1,600$ s. Grey symbols (data) and dashed lines (best fits) correspond to time controls (no shear applied). Inset, $J(t, t_w)$ (for $t_w \leq 1,600$ s) collapsed onto a master curve using the rescaled time with $\mu = 0.4$. **d**, Rejuvenation was quantified as the per cent change between $J(t, t_w)$ at $t = 1$ s, $t_w = 10$ s after shear, and the creep before shear, at $t = 1$ s (*significant changes between the two creep measurements, $p < 0.001$).

We assessed CSK remodelling through nanoscale bead motions arising from spontaneous structural rearrangements¹⁴. These motions showed intermittent dynamics with periods of confinement (stalling) punctuated by hops (Fig. 2). The mean square bead displacement (MSD) as a function of time lag Δt exhibited subdiffusive behaviour for small Δt and superdiffusive behaviour for large Δt (Fig. 3a). The subdiffusive regime was associated with stalling and the superdiffusive regime with hopping. This behaviour was quite general; human fetal lung fibroblasts, rat pulmonary vascular endothelial cells, and A549 epithelial cells showed similar dynamics, as did cells grown on micropatterned substrates on which they could adhere but not crawl (data not shown). By contrast, beads on locomoting cells show large diffusive or ballistic motions¹⁵.

The probability density function of bead displacements showed broad tails attributable to the hops (Fig. 3a, inset). This behaviour was quantified by the non-gaussian parameter α . The time lag Δt^* at which α reached its peak value was found to correspond to the transition between subdiffusive and superdiffusive behaviours (Fig. 3a,b). Intermittent dynamics and associated non-gaussian statistics are signatures of glassy systems^{7,16,17}, where slowing of dynamics and more prominent intermittency indicate approach of a glass transition and kinetic arrest^{7,18}.

We assessed proximity of the CSK to a glass transition as follows. As shown previously², over a wide frequency range the cell elastic modulus G' shows a weak power-law dependence on frequency, f , that is, $G'(f) \sim f^{x-1}$. As $x \rightarrow 1$, the system approaches purely elastic behaviour, and in soft glassy rheology theory, the system approaches a glass transition⁵. Taking x as a measure of proximity to a glass transition, we determined its value from $G'(f)$. As $x \rightarrow 1$, $\alpha(\Delta t^*)$ increased strongly (Fig. 3c), a behaviour reminiscent of colloidal systems approaching a glass transition, and indicative of approach to kinetic arrest^{7,18}. In the case of inert colloidal systems, Δt^* depends strongly on proximity to kinetic arrest and the MSD at longer times is a unique function of x (refs 18–20). In the case of cells, however, Δt^* showed a weaker dependence on x and did not seem to be determined solely by x (Fig. 3c, inset). Indeed, this point is underscored by closer examination of the MSD at long times; we fit the superdiffusive behaviour of the MSD to $D^*(\Delta t/t_0)^\beta$, where t_0 was arbitrarily taken to be 1 s. These responses did not show a unique relationship with x ; changes induced by variations in thermodynamic temperature followed a different relationship from those induced by drugs that modulate CSK structures, or those induced by depletion of intracellular ATP. Nonetheless, the closer the system was to a glass transition (smaller x), the slower were its dynamics (smaller D^* ; Fig. 3d) and the more non-gaussian its statistics (larger α ; Fig. 3c). These observations suggest that the rate of CSK rearrangements depends on the proximity of the glass transition as well as mechanical agitation driven by ATP-dependent force fluctuations.

To assess further the nature of forces that drive spontaneous bead motions, we first considered force fluctuations of purely thermal origin. We predicted the MSD using the generalized Stokes–Einstein relationship (GSER)²¹ and our measurements of the complex modulus $G^*(f)$. We focused on the local exponent, $\beta_{\Delta t}$ (where $\beta_{\Delta t} = \partial \log \langle r^2(\Delta t) \rangle / \partial \log \Delta t$, which tends to a constant value, denoted simply β , as Δt gets large). We compared this predicted exponent with that measured directly from spontaneous bead motions (Fig. 3a). Measurements approached the predictions from GSER for the smallest measured time lags, suggesting proximity to thermodynamic equilibrium (Fig. 4a). For longer times, however, predictions and data diverged, indicating a clear breakdown of GSER and establishing quantitatively appreciable departure of the system from thermodynamic equilibrium (in principle, the MSD should also show evidence of aging, but these studies were not designed to assess that possibility). However, when ATP in the cell was largely depleted, a closer correspondence between data and predictions was observed, and GSER breakdown was shifted to longer timescales.

We next considered active forces generated within the CSK. Lau *et al.*²² proposed that motor proteins cause significant force fluctuations within the CSK, and that the force–fluctuation power spectrum varies with frequency as $f^{-\lambda}$. In that case it can be shown that the exponent β characterizing spontaneous motions is related to the frequency exponent x characterizing CSK stiffness through $\beta = 2x + \lambda - 3$. Unlike any previous study in living cells, we had independent measurements of both $G^*(f)$ and MSD for each individual bead, and thus, depending on the hypothesized functional form $f^{-\lambda}$, we could evaluate λ quantitatively from measured values of x and β .

With thermal equilibrium, GSER requires $\lambda = 2 - x$, which implies $\beta = x - 1$. Our data are clearly inconsistent with this relationship (Fig. 4b). By contrast, Lau *et al.*²² further suggested fixing $\lambda = 2$, implying $\beta = 2x - 1$; this relationship fell in the vicinity of our observations where x was highest (Fig. 4b), and which corresponded to experimental conditions in which CSK structures are the most depolymerized²³ and the tension in the CSK network is smallest²⁴. But for smaller values of x , corresponding to conditions of a more polymerized CSK and greater contractile tension, observations and predictions diverged; the relationship $\beta = 2x - 1$ predicts that x and β must decrease together, whereas observations showed the opposite behaviour (Fig. 4b). The data suggest $\lambda = 2$ for the largest observed values of x , but $\lambda \approx 2.5$ for the smallest x . The value $\lambda = 2$ corresponds to force fluctuations that are finite but discontinuous, (that is, a series of force steps), whereas uniformly continuous force fluctuations would require $\lambda = 4$. Force spectra with exponents greater than two but substantially smaller than four correspond to smoothing of discontinuities in force steps over timescales that are short compared with measurement scales. Equivalently, this implies that forces exhibit temporal correlation (memory) or cooperativity. Importantly, if λ is allowed to vary with x (specifically as $\lambda = 2x - \beta - 3$), then the scale factor relating force fluctuations, stiffness, and spontaneous motion reduces to a frequency-independent number. That number could then be interpreted as a characteristic energy scale or, equivalently, an effective temperature^{8,25,26}. Confirmation of this hypothesis would require independent measurement of the force fluctuation spectrum, however, which to date is lacking.

A physical picture capturing these dynamics uses an energy landscape to describe all possible microconfigurations of the CSK. Thermal energy is typically insufficient to push the system over energy barriers into different microconfigurations; this is analogous to a jammed state^{27,28}. Through intermittent transitions from one metastable state to another, the system evolves slowly (ages) into more stable micro-configurations⁸. Imposed mechanical stress can provide sufficient energy to bring the system to a new microconfiguration, thus pushing the system farther

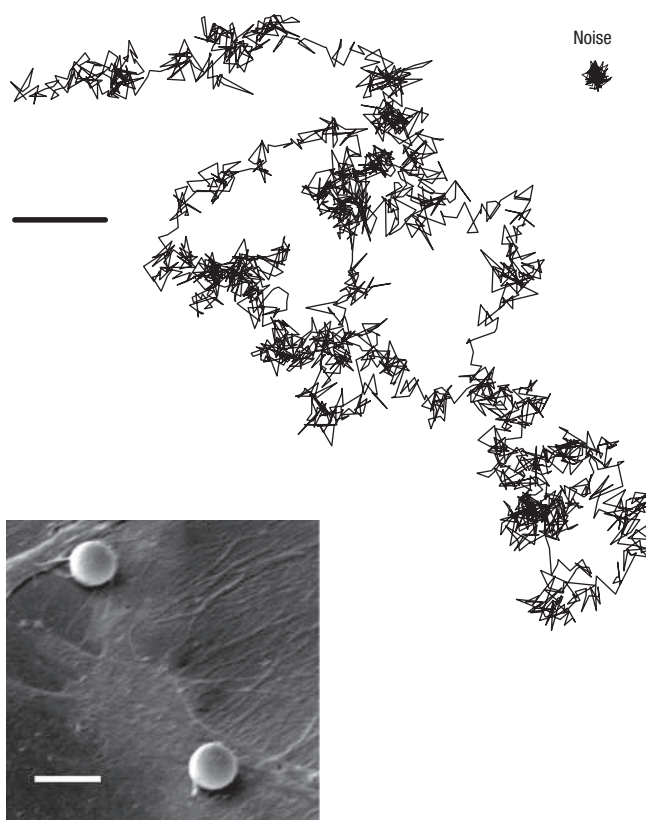


Figure 2 Bead position tracked in the plane. A representative bead on a cell shows intermittent dynamics. Scale bar = 10 nm. The trajectory of a bead glued to the coverslip represents the upper limit of measurement noise (upper right). Inset: Scanning electron microscopy (Carl Zeiss 1450VP SMT) of beads on HASM cells. Scale bar = 5 μm .

from thermodynamic equilibrium and resetting this evolution (rejuvenation). However, ATP-dependent rearrangements of the CSK modify the microconfigurations themselves, providing an alternate means of exploring new configurations; ATP hydrolysis can drive both protein conformational changes and polymerization/depolymerization cycles, either of which could conceivably resolve constraints and drive structural rearrangements. This is radically different from traditional glassy systems that remain trapped in a microconfiguration for increasingly long times because only thermal energy is available to allow the system to evolve. Nevertheless, the analogy between the behaviour of the living CSK and the behaviour of inert soft glassy systems is striking, and brings together into one picture elastic energy storage, mechanical energy dissipation, and structural rearrangements. These factors determine the extent to which cells exhibit fluid-like versus solid-like behaviour, with implications for all integrative cell functions that depends upon mechanical features.

Biological systems are increasingly being considered as highly interconnected maps of protein interactions, but even when such comprehensive maps become available, they may be insufficient to define biological function because they do not encompass principles that govern dynamics at intermediate (mesoscale) levels of organization^{29–31}. We propose here that trapping, intermittency, and approach to kinetic arrest are mesoscale features of CSK protein–protein interactions that link integrative phenotypic functions to underlying molecular events.

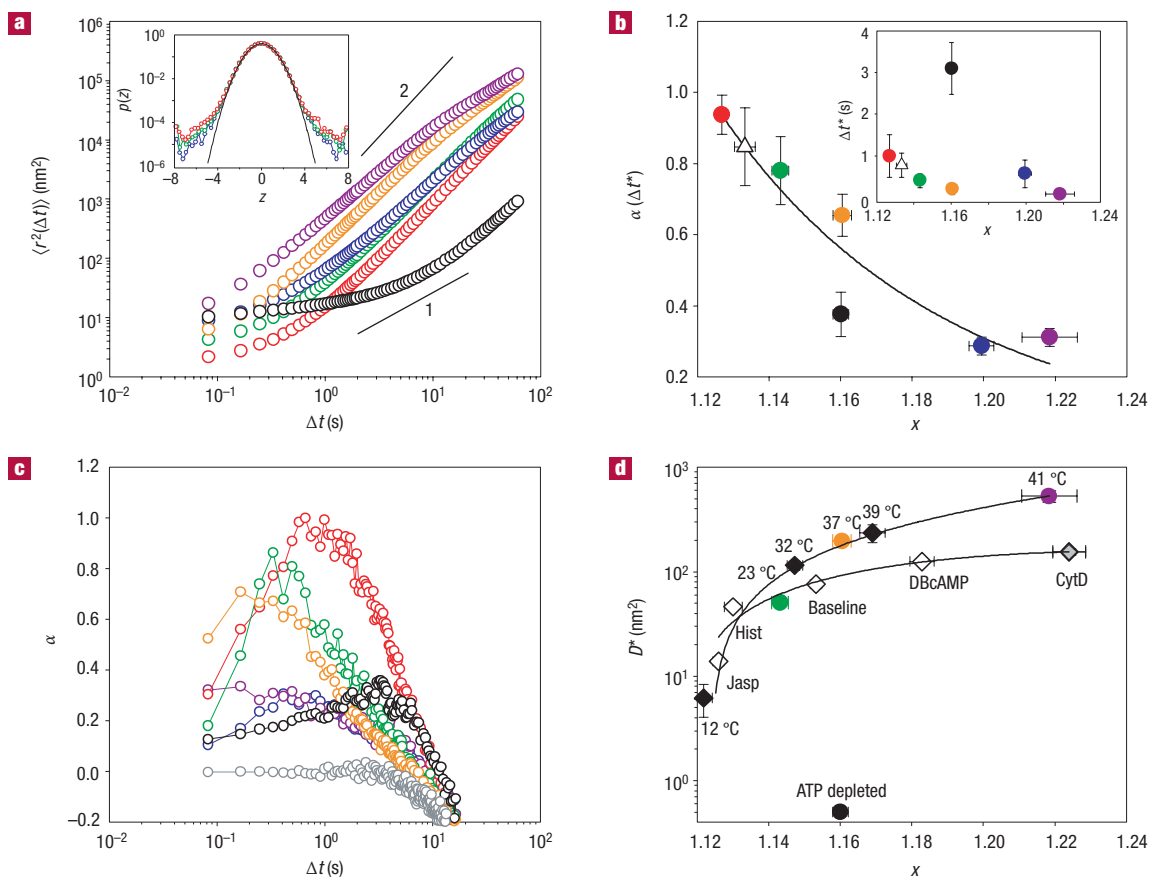


Figure 3 Statistics of spontaneous bead motions. **a**, MSD $\langle r^2(\Delta t) \rangle$ ($n = 400$ to 720 beads per group) versus time lag Δt . Groups are 23°C (green), 37°C (orange) and 41°C (purple), DbcAMP (blue), Jaspilakinolide (red), and ATP depletion (black). Solid lines indicate logarithmic slopes of 1 and 2. Inset, Probability density distribution $p(z)$ of one-dimensional normalized bead displacements z , shown for time lags Δt^* . Line is best-fit gaussian. The break from purely gaussian behaviour occurred at roughly $|z| = 4$. This is in contrast to the behaviour seen in colloidal systems¹⁹ where the break occurs at roughly $|z| = 2$. Compared with colloids, the hopping events in cells are far less frequent, but systematically much larger. **b**, Non-gaussian parameter α versus Δt . Colour coding the same as above, grey symbols represent beads glued to the coverslip. **c**, $\alpha(\Delta t^*)$ decreases with increase in x . Open triangles: cells in PBS plus glucose (10 mM) at 23°C . Inset, Δt^* versus x (bars in the x -direction are standard errors; bars in the y -direction are estimated from **b**). Colour coding same as above. **d**, Cytoskeletal rearrangements D^* increase with x for different ambient temperatures or after CSK manipulations. Baseline condition measured at room temperature before adding agonists (Baseline), histamine (Hist), and cytochalasin D (CytD).

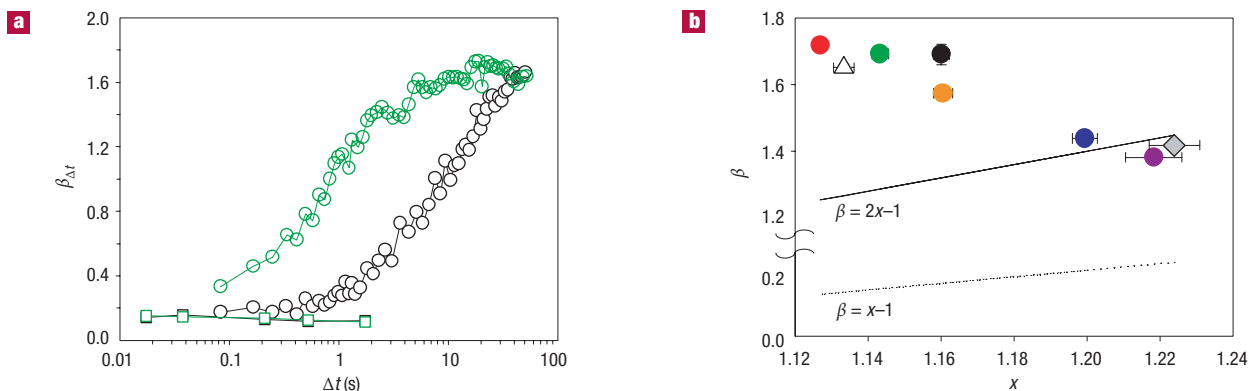


Figure 4 Physical forces involved in CSK rearrangements. **a**, Local slope $\beta_{\Delta t}$ (defined in text) determined from direct observations of $\langle r^2(\Delta t) \rangle$ (Fig. 3a) (circles) and from predictions based on GSER and measurements of $G^*(f)$ (squares). **b**, Exponent β measured from superdiffusive power-law regime of $\langle r^2(\Delta t) \rangle$ (symbols) and predictions if λ is taken to be equal to 2 universally as suggested by Lau *et al.*²² (solid lines) or predictions using GSER (dotted lines). Colour coding same as Fig. 3.

METHODS

EXPERIMENTAL PROTOCOL

HASM cells in passages 6–7 were serum-deprived for 24 h; serum deprivation arrests the cell cycle in the G_0/G_1 phases. Cells were harvested with trypsin and plated at 37 °C overnight in collagen-coated wells at a density of 20,000 cells per well. Ferrimagnetic beads (4.2 µm in diameter) were coated with a peptide containing the sequence Arg–Gly–Asp (RGD). These beads attach to HASM cells through integrin receptors and become strongly anchored to the CSK (Fig. 2, inset). Approximately 10,000 beads were added to an individual cell well and incubated for 20 min before the measurements. The experimental set-up and the measurement of elastic moduli are described elsewhere, as are local remodelling induced by the bead, the negligible effect of bead inertia, and technical limitations²⁴. The elastic modulus was fit to a power law over five decades of frequency f , with exponent $x-1$. x was modulated by treatment of the cell preparation with DBcAMP (decreases cell contractility, 1 mM), Jasplakinolide (stabilizes actin, 1 µM), histamine (increases cells contractility, 0.1 mM), and cytochalasin D (disrupts actin, 2 µM), changing the thermodynamic temperature, and depleting ATP. Note that the cytoskeletal modulations that we applied alter both macromolecular packing and the dynamics of crosslinked filament networks, and thus they cannot determine which of the two interactions plays the more dominant role.

CREEP FUNCTION

By imposing a uniform magnetic field (Fig. 1a), a small step torque of constant amplitude (volume specific torque of magnitude 42 Pa for 10 s duration) was applied to each bead and resulting bead motions deformed CSK structures deep in the cell interior²⁵. Ongoing bead displacements were expressed per unit applied specific torque, that is, as a creep function $J(t)$. The stiffer the cell, the smaller the displacement of the bead, and the smaller $J(t)$. Details of the method and technical limitations have been discussed elsewhere⁴.

AGING

We investigated aging at the cellular level using a novel microrheological approach (Fig. 1a). First, a small step torque was applied for 10 s to measure the creep function $J(t)$. Forty seconds after cessation of the step torque, a large oscillatory shear was produced by applying a large oscillatory torque (20 s, 1 Hz). The large oscillatory torque was then stopped, and after a waiting time t_w the creep function $J(t, t_w)$ was measured again for a wide range of t_w (from 10 s up to 8,000 s). As the dynamics of aging systems is ever evolving, aging experiments only make sense if system age t_w is measured starting from a reproducible initial state. To achieve a reproducible initial state, we followed shear-loading histories closely similar to those that have been used routinely in inert aging systems^{10,11}. Furthermore, cell wells were submitted to the exact same preparation history: 20 min of bead incubation, 5 min for preparation, then the protocol was launched; creep measurements were performed at identical times for both control and shear protocols. In both protocols, $t_w = 0$ is set 25 min after addition of the beads. Rejuvenation experiments were performed using the shear protocol.

ATP DEPLETION

ATP was depleted by incubation with 2 mM deoxyglucose and 2 mM NaN_3 . Residual ATP was assayed using a standard luciferase-based ATP determination kit (Sigma), and demonstrated that ATP concentrations after depletion were from 2–7% of that in control samples.

SPONTANEOUS BEAD MOTIONS

Spontaneous bead motions were measured by identifying the position of the centre of mass of each bead at the rate of 12 frames per second (0.082 seconds per frame) at $\times 40$ magnification for approximately 5 to 10 min. We defined bead displacement Δy as the distance travelled in direction y for each Δt , and the trajectory for each bead typically comprised 4,100–8,200 such displacements. Each bead displacement was normalized using its time averaged value $\overline{\Delta y}$ and its standard deviation STD^{23} ; normalized bead displacement z was calculated as:

$$z = \frac{(\Delta y - \overline{\Delta y})}{\text{STD}}$$

Because each experimental group typically comprised hundreds of bead–cell pairs, and taking into account the length of each record, each probability density function $p(z)$ of step sizes was therefore based on roughly 10^6 individual observations.

To quantify departures of the bead behaviour from gaussian statistics, we computed the non-gaussian parameter α from normalized displacements z as,

$$\alpha = \left(\langle z^4 \rangle / 3 \langle z^2 \rangle^2 \right) - 1$$

Brackets $\langle \rangle$ denote average over all beads in an experimental group. α is zero for a gaussian distribution and greater than zero when the distribution has broad non-gaussian tails⁷.

As an experimental control we measured $p(z)$ and α for beads that were glued to the coverslip (Fig. 3b). These observations showed almost perfect gaussian behaviour down to probabilities as small as 10^{-8} for z close to 6. At time lags for which α in cells showed peak values in the range 0.3 to 0.9, α for beads in glue was 30 times smaller.

We defined MSD as $\langle (r^2(\Delta t)) \rangle = \langle (r(t + \Delta t) - r(t))^2 \rangle$ where $r(t)$ is the bead position at time t , Δt is the time lag, and brackets indicate an average over t and over all beads. If the MSD goes as Δt^β , several behaviours emerge. For brownian motion (for example, diffusive movement of a microscopic sphere in a newtonian fluid), β is unity. If β is smaller than unity the motion is called subdiffusion, and when it is larger than unity the motion is called superdiffusion. When β is two, the motion is ballistic.

GSER

For a large spherical tracer at thermodynamic equilibrium, where dynamics are driven by the thermal forces alone, the GSER²¹ holds that $\langle r^2(\Delta t) \rangle$ is related to the complex modulus $G^*(f)$ by:

$$\langle r^2(\Delta t) \rangle = \zeta^{-1} \left(\frac{k_B T}{\pi a i f G^*(f)} \right)$$

where T is absolute temperature, k_B is Boltzmann's constant, a is probe diameter, $i^2 = -1$, and ζ^{-1} denotes the inverse Fourier transform. For a general material that displays temporal scale-free behaviour, $G^*(f)$ varies as $f^{\beta-1}$ with x between 1 (purely elastic) and 2 (purely viscous). In this case, GSER²¹ implies $\langle r^2(\Delta t) \rangle = c \Delta t^\beta$, where $\beta = x - 1$. Unlike the ideal case of a tracer in an infinite homogeneous medium, in our experiments the geometrical prefactor, c , depends on the extent of bead embedding into the cell and cell height. Thus, assessment of the prefactor c was substantially less certain than that of the local exponent β_{loc} , and its limiting value β .

Received 18 October 2004; accepted 25 April 2005; published 5 June 2005.

References

- Alcaraz, J. *et al.* Microrheology of human lung epithelial cells measured by atomic force microscopy. *Biophys. J.* **84**, 2071–2079 (2003).
- Fabry, B. *et al.* Scaling the microrheology of living cells. *Phys. Rev. Lett.* **87**, 148102 (2001).
- Desprat, N., Richert, A., Simeon, J. & Asnacios, A. Creep function of a single living cell. *Biophys. J.* **88**, 2224–2233 (2005).
- Lenormand, G., Millet, E., Fabry, B., Butler, J. & Fredberg, J. Linearity and time-scale invariance of the creep function in living cells. *J. R. Soc. Interface* **1**, 91–97 (2004).
- Sollich, P. Rheological constitutive equation for a model of soft glassy materials. *Phys. Rev. E* **58**, 738–759 (1998).
- Findley, W. N., Lai, J. S. & Onaran, K. *Creep and Relaxation of Nonlinear Viscoelastic Materials with an Introduction to Linear Viscoelasticity* (Dover Publications, Mineola, New York, 1989).
- Weeks, E. R., Crocker, J. C., Levitt, A. C., Schofield, A. & Weitz, D. A. Three-dimensional direct imaging of structural relaxation near the colloidal glass transition. *Science* **287**, 627–631 (2000).
- Parisi, G. Brownian motion. *Nature* **433**, 221 (2005).
- Struick, L. C. E. *Physical Aging in Amorphous Polymers and Other Materials* (Elsevier, Houston, Texas, 1978).
- Viasnoff, V. & Lequeux, F. Rejuvenation and overaging in a colloidal glass under shear. *Phys. Rev. Lett.* **89**, 065701 (2002).
- Derec, C., Ducouret, G., Ajdari, A. & Lequeux, F. Aging and nonlinear rheology in suspensions of polyethylene oxide-protected silica particles. *Phys. Rev. E* **67**, 061403 (2003).
- Ramos, L. & Cipelletti, L. Ultraslow dynamics and stress relaxation in the aging of a soft glassy system. *Phys. Rev. Lett.* **87**, 245503 (2001).
- Cloitre, M., Borrega, R. & Leibler, L. Rheological aging and rejuvenation in microgel pastes. *Phys. Rev. Lett.* **85**, 4819–4822 (2000).
- An, S. S. *et al.* Role of heat shock protein 27 in cytoskeletal remodeling of the airway smooth muscle cell. *J. Appl. Physiol.* **96**, 1701–1713 (2004).
- Kucik, D. F., Elson, E. L. & Sheetz, M. P. Forward transport of glycoproteins on leading lamellipodia in locomoting cells. *Nature* **340**, 315–317 (1989).
- Cipelletti, L. *et al.* Universal non-diffusive slow dynamics in aging soft matter. *Faraday Discuss.* **123**, 237–251 (2003).
- Bissig, H., Romer, S., Cipelletti, L., Trappe, V. & Schurtenberger, P. Intermittent dynamics and hyper-aging in dense colloidal gels. *Phys. Chem. Comm.* **6**, 21–23 (2003).
- Kob, W., Donati, C., Plimpton, S. J., Poole, P. H. & Glotzer, S. C. Dynamical heterogeneities in a supercooled Lennard-Jones liquid. *Phys. Rev. Lett.* **79**, 2827–2830 (1997).
- Weeks, E. R. & Weitz, D. A. Properties of cage rearrangements observed near the colloidal glass transition. *Phys. Rev. Lett.* **89**, 095704 (2002).
- Evans, R. M. L., Cates, M. E. & Sollich, P. Diffusion and rheology in a model of glassy materials. *Eur. Phys. J.* **10**, 705–718 (1999).
- Mason, T. G. & Weitz, D. A. Optical measurements of frequency-dependent linear viscoelastic moduli of complex fluids. *Phys. Rev. Lett.* **74**, 1250–1253 (1995).
- Lau, A. W. C., Hoffman, B. D., Davies, A., Crocker, J. C. & Lubensky, T. C. Microrheology, stress fluctuations, and active behavior of living cells. *Phys. Rev. Lett.* **91**, 198101 (2003).
- An, S. S., Laudadio, R. E., Lai, J., Rogers, R. A. & Fredberg, J. J. Stiffness changes in cultured airway smooth muscle cells. *Am. J. Physiol. Cell Physiol.* **283**, C792–C801 (2002).
- Stamenovic, D., Suki, B., Fabry, B., Wang, N. & Fredberg, J. J. Rheology of airway smooth muscle cells is associated with cytoskeletal contractile stress. *J. Appl. Physiol.* **96**, 1600–1605 (2004).
- Kurchan, J. In and out of equilibrium. *Nature* **433**, 222–225 (2005).
- Cugliandolo, L. F., Kurchan, J. & Peliti, L. Energy flow, partial equilibration, and effective temperature in systems with slow dynamics. *Phys. Rev. E* **55**, 3898–3914 (1997).
- Trappe, V., Prasad, V., Cipelletti, L., Segre, P. N. & Weitz, D. A. Jamming phase diagram for attractive particles. *Nature* **411**, 772–775 (2001).
- Liu, A. J. & Nagel, S. R. Jamming is not just cool any more. *Nature* **396**, 21–22 (1998).
- Kitano, H. Systems biology: a brief overview. *Science* **295**, 1662–1664 (2002).
- Csete, M. E. & Doyle, J. C. Reverse engineering of biological complexity. *Science* **295**, 1664–1669 (2002).
- Noble, D. Modeling the heart—from genes to cells to the whole organ. *Science* **295**, 1678–1682 (2002).
- Hu, S. *et al.* Intracellular stress tomography reveals stress focusing and structural anisotropy in cytoskeleton of living cells. *Am. J. Physiol. Cell Physiol.* **285**, C1082–C1090 (2003).
- Valentine, M. T. *et al.* Investigating the microenvironment of inhomogeneous soft materials with multiple particle tracking. *Phys. Rev. E* **64**, 061506 (2001).

Acknowledgements

These studies were supported by the National Institutes of Health, grants HL33009, HL59682 and HL65960. We thank Reynold Panettieri for providing cells and Srboljub M. Mijailovich, John C. Crocker and Steven S. An for helpful discussions.

Correspondence and requests for materials should be addressed to J.J.F.

Competing financial interests

The authors declare that they have no competing financial interests.